Ensemble EMD-based automatic extraction of the catenary structure wavelength from the pantograph-catenary contact corce

Liu, Zhigang; Wang, Hongrui; Dollevoet, Rolf; Yang, Song; Nunez Vicencio, Alfredo; Zhang, Jingyu

DOI
10.1109/TIM.2016.2579360

Publication date
2016

Document Version
Accepted author manuscript

Published in
IEEE Transactions on Instrumentation and Measurement

Ensemble EMD-Based Automatic Extraction of the Catenary Structure Wavelength from the Pantograph-Catenary Contact Force

Zhigang Liu, *Senior Member*, *IEEE*, Hongrui Wang, *Student Member*, *IEEE*, Rolf Dollevoet, Yang Song, *Student Member*, *IEEE*, Alfredo Núñez, *Senior Member*, *IEEE*, Jing Zhang

***Abstract*—This paper explores the use of pantograph-catenary contact force (PCCF) for monitoring of the current collection quality and detection of anomalies in the interaction between pantograph and catenary. The concept of catenary structure wavelength (CSW) is proposed as the dominant component of PCCF. It describes the signal components caused by the cyclical catenary structure in span and inter-dropper distance. To obtain the CSWs and non-CSW residual of PCCF, an automatic extraction approach based on the ensemble empirical mode decomposition (EEMD) is proposed. In the approach, the instantaneous frequency of each intrinsic mode function generated by EEMD is employed for the extraction of CSWs. Some selected trials on the PCCF data from simulation and measurement are performed and indicate that the extraction approach is adaptive to the PCCF under various circumstances, including different operation speed, pantograph type and catenary structure. Analyses on the extracted CSWs and non-CSW residual show that, with certain tolerance against measurement noise, the approach can preserve intact the characterizations of current collection quality and make anomalies easier to detect.**

***Index Terms*—High-speed railway, pantograph-catenary contact force (PCCF), catenary structure wavelength (CSW), ensemble empirical mode decomposition (EEMD), intrinsic mode function (IMF), extraction.**

I. Introduction

IN RECENT years, the high-speed railway (HSR) industry is expanding extensively all over Europe, Asia, Oceania and North America for promising economic benefit and social development [1], [2]. The assuring safe operation of railway rolling stock at high speed is the very foundation and the major advantage of HSR. To ensure the stability of HSR along with the continuous increase of train speed, the dynamic performance of the entire HSR system should be improved simultaneously. One of the most critical dynamic performance indexes is the quality of the current collection of the high-speed locomotives, which measures the efficiency in the transmission of the power from the catenary to the locomotive. The pantograph-catenary sliding contact above the locomotive roof determines the quality of current collection to a great extent. However, considering the flexibility and nonlinearity of catenary suspension [3], the pantograph-catenary sliding contact is relatively vulnerable to the excitations caused by anomalies. Currently, with the higher operation speeds leading to higher oscillations of catenary suspension [4], the pantograph-catenary interaction requires significant attention now more than ever. It is one of the key components that limit the speed upgrade of HSR. It requires an optimal design and efficient operation and maintenance as a whole system, together pantograph and catenary.

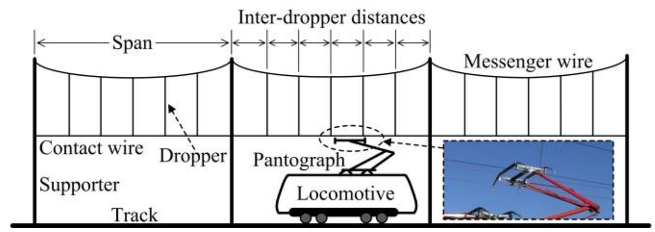

Fig. 1. Schematic of the pantograph-catenary system.

Mechanically, as the crucial and required measurement data that reflects the pantograph-catenary sliding contact [5], the pantograph-catenary contact force (PCCF) must be maintained in an acceptable range during operation [6]; otherwise, arcs [7] or severe wear [8] will occur. The PCCF normally contains certain waveforms that characterizes the periodicity of the catenary structure despite of the pantograph type. As schematically shown in Fig. 1, the catenary suspension is mainly composed of the contact wire, messenger wire, dropper, supporter, and so on. In an anchoring section, the tension that can be exerted on the both ends of contact wire or messenger wire is finite. To maintain the contact wire in an adequate position, the catenary is constructed as the cyclical structure shown in Fig. 1. Thus, the nominal configuration of a catenary suspension is strictly periodic if the span and inter-dropper distances are uniform in an anchoring section [9]. In practice, although the actual configuration of catenary suspension is inevitably distorted compared with design, the periodicity can

This work was supported in part by the National Natural Science Foundation of China under Grant U1434203, 51377136 and 51405401, in part by the Sichuan Province Youth Science and Technology Innovation Team under Grant 2016TD0012, and in part by the China Scholarship Council under Grant 201507000029. *(Corresponding author: Hongrui Wang.)*

Z. Liu, Y. Song and J. Zhang are with the School of Electrical Engineering, Southwest Jiaotong University, Chengdu 610031, China (e-mail: liuzg@swjtu.cn; gabrielleyy@163.com; zhangjing79@home.swjtu.edu.cn).

H. Wang is with the School of Electrical Engineering, Southwest Jiaotong University, Chengdu 610031, China and the Section of Railway Engineering, Delft University of Technology, 2628CN Delft, The Netherlands (e-mail: soul_wang0@163.com).

R. Dollevoet and A. Núñez are with the Section of Railway Engineering, Delft University of Technology, 2628CN Delft, The Netherlands (e-mail: R.P.B.J.Dollevoet@tudelft.nl; A.A.NunezVicencio@tudelft.nl).

still be generally remained.

Consequently, in previous studies concerning pantograph-catenary interaction, the periodicity of catenary structure can be constantly identified in the PCCF signals from either simulation results or real-life measurements. In order to investigate the frequency-domain characteristics of PCCF, the Fourier transform and the power spectrum density are frequently adopted [10]-[15]. As a result, the frequency components that characterize the span and inter-dropper distance can be observed from the frequency domain of PCCF. Thus, in this paper, the term Catenary Structure Wavelength (CSW) is proposed to represent all the signal components caused by the cyclical structure of the soft catenary.

To the best of our knowledge, the CSWs inevitably exist in PCCF as long as the soft catenary suspension is adopted for the purpose of power transmission in HSR. In fact, due to the variation of contact wire elasticity along the catenary, the CSWs generally occupy a large proportion of energy in PCCF, which makes other signal components that may be caused by anomalies such as contact wire irregularity [14], contact strip wear [16], environmental perturbation [17], etc. almost unobservable. Therefore, the extraction of the CSWs in PCCF can be useful in the following two aspects:

1) The obtained CSWs are the dominant signal components in PCCF, which can reveal the overall trend and fluctuation of PCCF. Also, the CSWs are highly sensitive to the positional deviations occurred in catenary structure. Thus, the CSWs can be used to evaluate the overall quality of pantograph-catenary interaction.

2) With the elimination of CSWs, the residual is the PCCF containing the signal components that are caused by all other factors except for the catenary structure. In the residual, all the anomalies that may exist in the pantograph and catenary or occur in the pantograph-catenary interaction will be contained.

Therefore, this paper aims to develop a generic filtering approach to extract the CSWs in PCCF. Considering the variety of catenary structure, pantograph type, measuring method and measurement condition in different areas and scenarios, the extraction should be adaptive to any PCCF measurement data. The required prior information are simply the ranges of span and inter-dropper distance in the measured catenary structure, which can also be substituted by the commonly designed ranges of the two distances. Regarding to the extraction of specific frequency components in a multicomponent signal, the well-known Fourier transform [18] and wavelet transform [19] are potential candidates. However, the major frequency components of PCCF shift as the catenary structures are diverse for different railway lines. Even for the same railway line, the catenary structure is not absolutely uniform and consistent along the entire line. If the Fourier transform or wavelet transform were adopted in this case, the major frequency components need to be identified prior to the decomposition of PCCF, which is difficult to implement when dealing with signal segments from a large dataset and sometimes with unavailable measurement condition. Addressing this issue, with the invention of empirical mode decomposition (EMD) [20], the self-adaptive decomposition of multicomponent signal provides a more suitable way for the purpose of CSW extraction. Theoretically, EMD can decompose a PCCF signal into several intrinsic mode functions (IMFs), which automatically sifts out the major frequency components in the signal, regardless of the various sources of PCCF. That is to say, the generated IMF itself might be the exact CSW if the EMD is properly performed on the PCCF signal. In this case, using the enhanced EMD, i.e. the ensemble EMD (EEMD) [21], the CSW extraction is automatically realized as an extension for the convenience of anomaly detection in PCCF analysis [22]. It can filter out the CSWs in PCCF and facilitates further developments in the efficient design of maintenance strategies for the pantograph-catenary system.

TABLE I
PARAMETERS OF THE SIMPLE CATENARY MODEL

Type		Value	Type		Value
Span		48m	Encumbrance		1.6m
Installation height		5.3m	Stagger		±0.2m
Contact wire	Tension	27kN	Total distance		14 spans
	Line density	1.07kg/m	Maximum pre-sag of contact wire		5‰Span
	Tensile rigidity	10^6N/m	Number of droppers per span		5
Messenger wire	Tension	21kN	Element length		0.125m
	Line density	1.07kg/m	Dropper	Line density	0.14kg/m
	Tensile rigidity	10^6N/m		Tensile rigidity	10^5N/m
Inter-dropper distances in a span		5m/9.5m/9.5m/9.5m/9.5m/5m			

The rest of the paper is organized as follows. A theoretical description of the CSW is given in detail in Section II. The automatic extraction approach for the CSWs is proposed and illustrated in Section III. Section IV presents some validations and possible applications with the results from the extraction approach. The conclusions are drawn and some future developments are suggested in Section V.

II. THE CONCEPT OF CSW

Given a proper height of contact wire and initial force acting on the contact wire from a pantograph, the pantograph-catenary system can be functional during a long-distance and high-speed

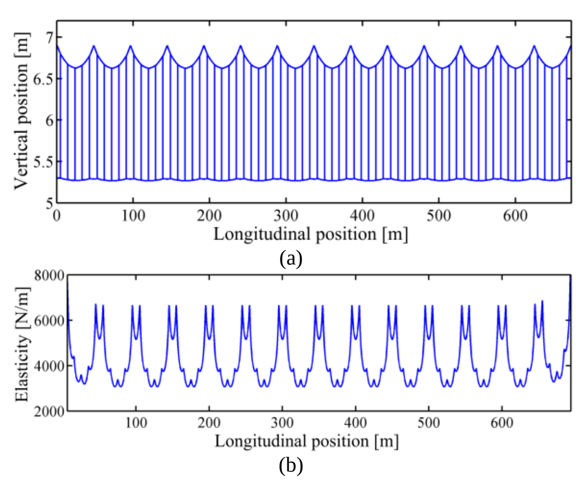

Fig. 2. (a) Initial configuration of the simple catenary model. (b) The contact wire elasticity under 100N static force.

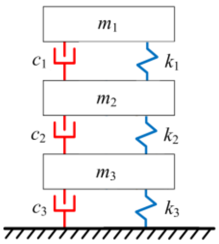

(b)

Fig. 3. The three-level lumped mass model of pantograph.

TABLE II
THE PHYSICAL PARAMETERS OF PANTOGRAPHS

Parameter	Pantograph type	
	DSA380	SSS400+
m_1 (kg)	7.12	6.05
m_2 (kg)	6.0	6.4
m_3 (kg)	5.8	14
k_1 (N/m)	9430	5813
k_2 (N/m)	14100	13600
k_3 (N/m)	0.1	0
c_1 (Ns/m)	0	0
c_2 (Ns/m)	0	0
c_3 (Ns/m)	70	64.9

operation. The sliding contact between the contact wire and the pantograph is maintained through the PCCF. To introduce the concept of CSW to PCCF, a brief demonstration of the CSWs is given below by adopting the catenary modelling approach proposed in [3], which is previously verified according to the European Standard EN 50318 [23] and the recent pantograph-catenary simulation benchmark summarized in [24].

The ideal configuration of a simple catenary model, which adopts the actual structure parameters of the Beijing-Tianjin HSR line in China given in Table I, is shown in Fig. 2(a). As expected, the periodicity of catenary structure can be observed. Since the pantograph-catenary sliding contact is partly depending on the geometric configuration of catenary, the PCCF should have a correlation with the static contact wire height especially under high speed [15]. From another perspective, by applying a static vertical force on each point of the contact wire, the elasticity of the contact wire can be calculated as the ratio of the force vs. the vertical displacement of the contact point. As a result, the contact wire elasticity of the catenary model is obtained and depicted in Fig. 2(b). It can be concluded that, not only the geometry of the catenary, but also the response of the contact wire under the action of static force shows certain periodicity in spans and inter-dropper distances.

Combing the catenary model with the three-level lumped mass model of pantograph depicted in Fig.3, which contains three lumped masses m_1, m_2 and m_3 representing the head, frame and bottom of the pantograph respectively, and three spring-damper elements between adjacent masses and m_3 and the ground, the PCCF can be computed using the frequently adopted penalty function method as follows.

$$\begin{cases} F(k) = K_c(u_p(k) - u_c(k)) & u_p(k) \geq u_c(k) \\ F(k) = 0 & u_p(k) < u_c(k) \end{cases} \quad (1)$$

where $F(k)$ is the PCCF at the k th sampling point, $u_p(k)$ and $u_c(k)$ are the vertical position of pantograph and contact wire at the sampling point, respectively, and K_c is the contact stiffness between pantograph and catenary, which is 82300N/m for this model. It can be seen that the PCCF is proportional to the penetration depth that is calculated partly based on the contact wire height. During an ideal operation with no contact loss, the PCCF at each sampling point is depending on the periodic variation of contact wire height, where the periodicity is introduced to the PCCF directly.

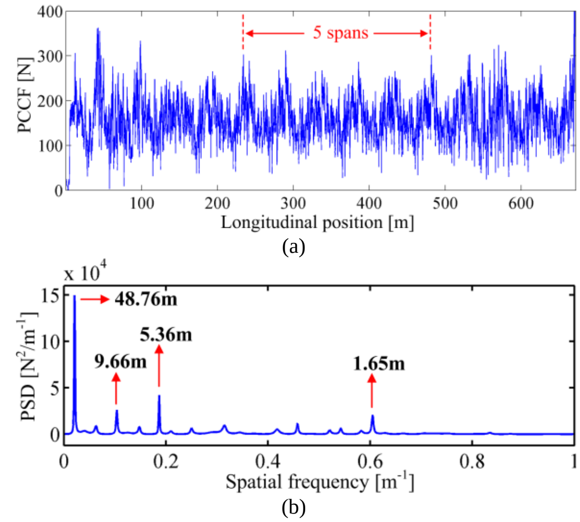

Fig. 4. (a) The computed PCCF signal and (b) its power spectrum density.

Furthermore, Table II provides the physical parameters of two types of high-speed pantograph in China. The PCCF combining the simple catenary model and the DSA380-type pantograph under the operation speed of 300km/h is computed and depicted in Fig. 4(a). The sampling interval of PCCF is equal to the element length of contact wire so that no interpolation is performed during the computation. Due to the boundary effect at both ends of the catenary model, the PCCF is unstable in the first and last several spans. Thus, the PCCF in the middle 5 spans indicated by the red lines in Fig. 4(a) is selected for further analysis. From the power spectrum density of selected PCCF signal depicted in Fig. 4(b), the frequency components, i.e. the wavelength components that are reflected by the significant peak energies are obtained. Comparing with the structure parameters of catenary, it is straightforward to identify the wavelength components 48.76m, 9.66m and 5.36m as the representation of the span and inter-dropper distances, which is a common phenomenon in frequency-domain PCCF analysis. In particular, the wavelength components are almost identical with those in [22] where a different modeling approach is realized based on the same structure parameters of catenary and pantograph. Here, the term CSW is used to characterize the wavelengths caused by spans and inter-dropper distances. Like shown in Fig. 4(b), the CSWs are generally the dominant components in a normal or healthy PCCF signal, which endows the CSWs and the non-CSW PCCF with different but significant physical meanings. Hence, based on the concept of CSW, this study focuses on the extraction of CSWs for facilitating the evaluation of current collection quality and the detection of anomalies.

III. EEMD-Based CSW Extraction

A. *EMD Algorithm*

EMD is a data-driven algorithm that adaptively decomposes a signal into several modes based on neither sinusoidal functions nor mother wavelet functions but the IMFs of the signal itself. Despite of the lack of theoretical support [25], EMD has been widely used in many applications where signal

Please cite as: Z. Liu, H. Wang, R. Dollevoet, Y. Song, A. Núñez, J. Zhang, “Ensemble EMD-based automatic extraction of the catenary structure wavelength from the pantograph-catenary contact force”. Accepted IEEE Transactions on Instrumentation and Measurement, Jun. 2016. DOI: 10.1109/TIM.2016.2579360

decomposition is needed [26]-[29]. In some previous studies [30], [31], it is specifically adopted to eliminate the useless or noisy components of a signal. However, the extraction approach in this paper considers both the CSWs and the non-CSW PCCF useful components.

In brief, EMD decomposes a given signal $x(t)$ into a number N of IMFs $d_j(t)$, $j=1,2,...,N$ and a residual $r(t)$. The sum of all IMFs and the residual matches the original signal perfectly as follows.

$$x(t)=\sum_{i=1}^{N} d_j(t)+r(t) \tag{2}$$

where each IMF $d_j(t)$ is obtained through an iterative sifting process. For the first IMF $d_1(t)$, starting with a corresponding estimated IMF $d_1^{(i)}(t)$ where the iteration number $i=1$ and the estimated IMF $d_1^{(1)}(t)=x(t)$, the sifting iteration is described in five steps as follows.

Step 1: Find all the maxima and minima of the signal $d_1^{(i)}(t)$.

Step 2: Connect all the adjacent maxima and minima respectively using spline interpolation to form an upper and a lower envelope $e_u(t)$ and $e_l(t)$ of signal $d_1^{(i)}(t)$.

Step 3: Compute the mean of upper and lower envelopes $e_m(t)=\left[e_u(t)+e_l(t)\right]/2$.

Step 4: Update the estimated IMF $d_1^{(i+1)}(t)=d_1^{(i)}(t)-e_m(t)$ and the number of iterations $i=i+1$.

Step 5: Repeat Step 1 to Step 4 until a stopping criterion has been satisfied so that the first IMF $d_1(t)=d_1^{(i)}(t)$.

For other IMFs $d_j(t)$, $j>1$, the corresponding estimated IMF $d_j^{(i)}(t)$ for their first sifting in Step 1 should be

$$d_j^{(1)}(t)=x(t)-\sum_{k=1}^{j-1} d_k(t). \tag{3}$$

The conventional stopping criterion in Step 5 for each IMF at its i th iteration can be computed by the standard deviation computed as

$$SD(i)=\sum_{t=0}^{T}\frac{|d_j^{(i)}(t)-d_j^{(i-1)}(t)|^2}{|d_j^{(i-1)}(t)|^2}<\varepsilon \tag{4}$$

where ε is a positive number typically ranges from 0.2 to 0.3 [20] and T is the time duration of signal $x(t)$. The last output of the algorithm is actually the final residual $r(t)$ that represents the mean trend of signal $x(t)$.

From the algorithm above, it can be speculated that the number of IMFs N is automatically determined by the signal itself and the value ε in stopping criterion. As a result of the empirical algorithm, the IMFs have proved to be approximately zero-mean and both amplitude and frequency modulated. Moreover, due to smoothing effect of iterative sifting, the IMFs possess lower and lower frequencies as they are produced one after another. Thus, it is possible for EMD to directly extract the major frequency components in a multicomponent signal, e. g. the PCCF.

B. EEMD Algorithm

As groundbreaking as it is, the conventional EMD still has some shortcomings. In particular, the mode mixing problem caused by signal intermittency leads to frequency aliasing in the IMFs, which mixes disparate signal oscillations into IMFs and impairs the physical meaning of each IMF. However, the physical meaning of PCCF must be preserved in order to obtain authentic CSWs. To resolve this problem, EEMD is proposed based on the dyadic property of EMD when dealing with white noise [21]. It utilizes additional white noise to ensure the full physical meaning of IMFs as described in the following four steps.

Step 1: Add a random white noise series with constant standard deviation σ to the signal $x(t)$ to form a new signal.

Step 2: Perform the EMD on the new signal to get a set of IMFs.

Step 3: Repeat Step 1 and Step 2 for a number M of times.

Step 4: Compute the final IMFs by averaging all the M sets of IMFs correspondingly.

The added white noises preserve the disparate signal oscillations during every EMD and automatically cancel each other through the averaging in Step 4, so that the final IMFs are not contaminated by the white noises. Note that the final number of IMFs might be different from EMD result due to the added white noise, which is close to $\log_2(P)$ with P the number of total sample points. Comparing with the EMD, two new parameters are introduced to the EEMD algorithm, namely the standard deviation of the added white noise σ and the number of ensemble members M. Both parameters should be carefully chosen as they are relevant to the quality of the final IMFs. Specifically, σ normally ranges from 0.1 to 0.5 times the standard deviation of a given signal $x(t)$, and M can be from 10 to 100 depending on the tradeoff between the effect of white noise cancelation and the requirement of computational efficiency.

With the extracted IMFs from EMD or EEMD, the Hilbert-Huang Transform (HHT) is developed based on the concept of instantaneous frequency, which can provide the Hilbert spectrum of original signal in an energy-time-frequency distribution (TFD) [20]. Concretely, the analytic form of each IMF can be obtained using the Hilbert transform as follows.

$$z_j(t)=d_j(t)+\mathrm{i}H[d_j(t)]=a_j(t)\mathrm{e}^{\mathrm{i}\theta_j(t)} \tag{5}$$

where $H[d_j(t)]$ denotes the Hilbert transform of the j th IMF $d_j(t)$ and

$$\begin{cases} a_j(t)=\sqrt{d_j{}^2(t)+H[d_j(t)]^2} \\ \theta_j(t)=\arctan\left(\dfrac{H[d_j(t)]}{d_j(t)}\right) \end{cases}. \tag{6}$$

The instantaneous frequency is defined as

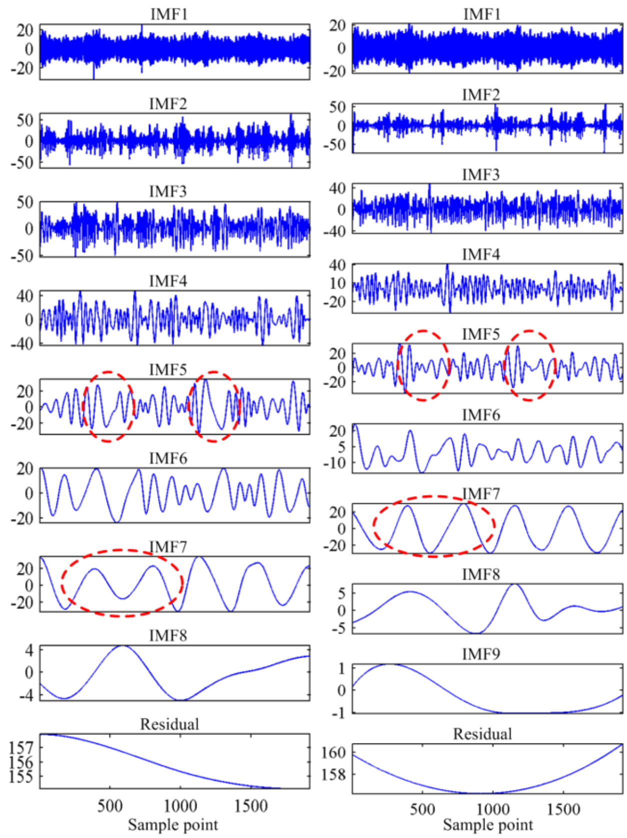

Fig. 5. IMFs generated by (a) EMD and (b) EEMD with σ=0.2 and $M=100$.

$$\omega_j(t)=\frac{\mathrm{d}\theta_j(t)}{\mathrm{d}t}. \quad (7)$$

Then the Hilbert spectrum of the signal $x(t)$ can be computed by

$$S(\omega,t)=\mathrm{Re}[\sum_{j=1}^{N}a_j(t)e^{\mathrm{i}\int\omega_j(t)dt}] \quad (8)$$

where Re denotes the real part of a complex signal. The Hilbert spectrum reveals the physical meaning of non-stationary data by computing the energy of the instantaneous frequency at each time instant, which shows favorable physical relevancy and high time-frequency resolution in many cases [32]. Thus, it is utilized to quantify and observe the physical meanings of IMFs of PCCF in the following section.

C. EEMD-Based Extraction Approach

Using the PCCF signal adopted for power spectrum density analysis in Fig. 4(a) as an example, both EMD and EEMD are directly performed and the generated IMFs are depicted in Fig. 5(a) and Fig. 5(b), respectively. Despite that EEMD generates one more IMF than EMD, it can be observed that the first to the seventh IMFs from the two approaches share the similar time-domain waveforms and declines in frequency ranges in the same manner. Among the IMFs, the fifth and seventh IMFs are notable for potential physical meanings that correspondingly indicate the CSWs. Specifically, both seventh IMFs show obvious periodicity in span cycles but local

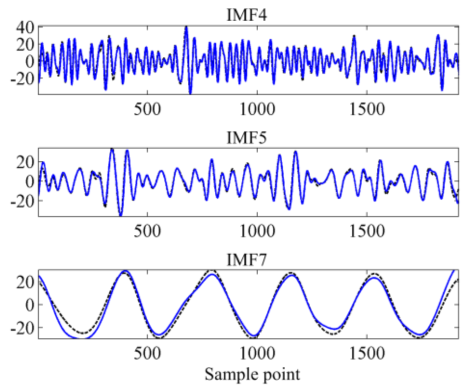

Fig. 6. IMFs generated by EEMD with (solid lines) and without (dashed lines) boundary extension.

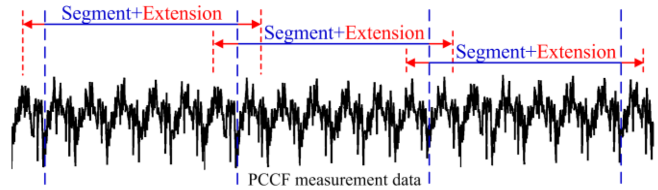

Fig. 7. Boundary extensions on the segments of a long-duration measurement data.

difference in amplitude as circled by dashed lines in the figure. The seventh IMF from EEMD possesses more complete and continuous waveform than the one from EMD. Likewise, the fifth IMF from EMD shows certain sign of intermittency as circled by the dashed lines, which can be regarded as the mode mixing phenomenon. Nevertheless, the corresponding IMF from EEMD effectively alleviates the phenomenon as expected.

Meanwhile, another common problem that occurs during the decompositions is the boundary effect. In the two sets of IMFs depicted in Fig. 5(a) and Fig. 5(b), the fourth to the seventh IMFs show signs of boundary effects at both ends of the waveforms, which means that partial signals at the ends are somewhat distorted comparing with those in the middle. To solve the problem, the simulation data outside of the 5-span duration is used as the boundary extension for the PCCF signal. In this case, the actual PCCF signal for EEMD is extended by the 200 adjacent sample points, namely about half a span at both ends of the 5-span signal. Comparisons between the corresponding IMFs that are obtained with and without boundary extension are depicted in Fig. 6. It can be seen that for the fourth, fifth and seventh IMFs, the general signal oscillation remain the same after boundary extension, whereas some amplitudes, especially at the ends are mildly modified by the extensions.

In the case of real-life measurements, because the PCCF signal adopted for decomposition is normally a segment of a long-duration PCCF measurement data, the boundary extension can still be achieved by using the contiguous sample points besides the segment. An illustration of the boundary extension on a PCCF measurement data is shown in Fig. 7. The duration of PCCF signal segment should be larger than 3 spans to reflect its periodicity in spans and less than 10 spans (or a larger number of spans depending on the sampling interval) for high computational efficiency. Meanwhile, the length of boundary

Please cite as: Z. Liu, H. Wang, R. Dollevoet, Y. Song, A. Núñez, J. Zhang, “Ensemble EMD-based automatic extraction of the catenary structure wavelength from the pantograph-catenary contact force”. Accepted IEEE Transactions on Instrumentation and Measurement, Jun. 2016. DOI: 10.1109/TIM.2016.2579360

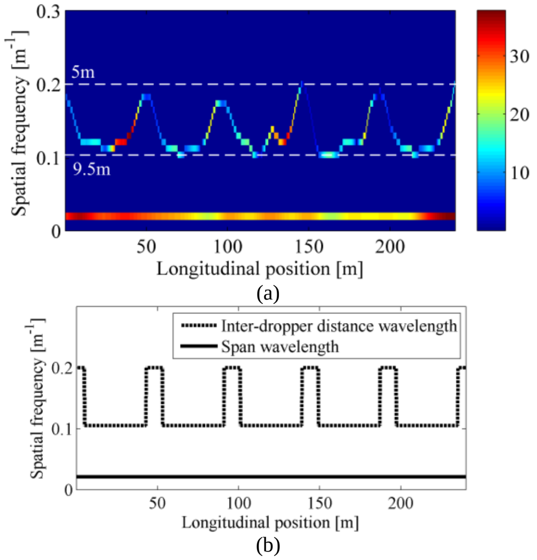

Fig. 8. (a) Hilbert spectrum of the fifth and seventh IMFs comparing with (b) the TFD of physical structure wavelengths of corresponding catenary.

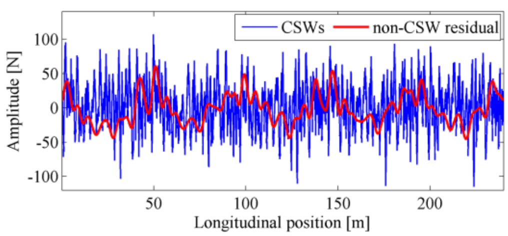

Fig. 9. Extracted CSWs and non-CSW residual from the PCCF signal.

extension should be at least half a span to preserve the integrity of the span wavelength at the boundary of a signal segment.

After the decomposition, the CSWs need to be recognized from all IMFs to accomplish the extraction. The HHT provides the frequency-domain information of all IMFs, which can identify the different frequency range of each IMF. Thus, the CSWs with specific frequency characteristic can be recognized correspondingly. From the above, it is presented that there are two CSWs, namely the span and inter-dropper distance wavelengths, in the decomposed PCCF signal. After applying HHT on all IMFs, the Hilbert spectrum of the fifth and seventh IMFs are selected and depicted in Fig. 8(a). Confirming the physical meanings of the two CSWs, the corresponding wavelengths are clearly shown in the figure. In detail, the span wavelength component at around 0.02m^{-1} is constant and continuous along the longitudinal direction, which occupies the dominant energy in PCCF. The other wavelength component oscillates between the dashed lines corresponding to 5m and 9.5m wavelengths with a certain pattern, which matches to the distribution of the inter-dropper distance in each span given in Table I. For comparison, the ideal TFD of the actual catenary structure is computed based on corresponding longitudinal position and depicted in Fig. 8(b). Although the PCCF is the dynamic reflection of catenary structure, its TFD is unlikely to be strictly identical to the TFD of static structure and may deviates due to the dynamic interaction. Thus, it can be speculated that, within a reasonable range, both CSWs are properly reflected by the spectrum and confirming to the actual structure parameters of catenary. As a result, the sum of the

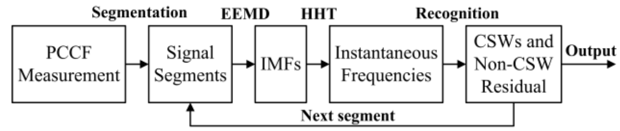

Fig. 10. Block diagram of the automatic CSW extraction approach.

fifth and seventh IMFs representing the CSWs and the rest of IMFs representing the non-CSW residual are depicted in Fig. 9. While the non-CSW residual shows no indication of significant regularity, it should be noted that the waveform of CSWs is highly similar to the variation of the contact wire elasticity given in Fig. 2(b), which validates the extraction result.

To realize the extraction process automatically, the frequency range of each IMF can be obtained by (7) and adopted for frequency recognition. More specifically, the structure parameters of catenary is variable but within a certain range. Generally, the span is between 40m and 70m and the inter-dropper distance is between 4m and 10m. Hence, the IMF with the instantaneous frequency ranges from 0.1m^{-1} to 0.25m^{-1} or 0.014m^{-1} to 0.025m^{-1} can be recognized as the inter-dropper distance wavelength or span wavelength respectively. Based on (7), the recognition on whether the j th IMF is a CSW can be judged by a Boolean variable

$$\Delta_j = \max[\omega_j(t)] < \omega_u \wedge \min[\omega_j(t)] > \omega_l \tag{9}$$

where $\wedge$ denotes logical conjunction and ω_u and ω_l are the upper and lower boundary for a certain CSW respectively. Since the signal decomposition based on EEMD and boundary extension can avoid the mode mixing problem between IMFs and ensure the validity of frequency segmentation of PCCF, the automatic recognition process is theoretically feasible. To sum up, Fig. 10 depicts the block diagram of the automatic extraction approach, which is performed on several examples in the following section. Note that in the step of EEMD, the corresponding boundary extension must be performed on the signal segment beforehand.

IV. Validation and Potential Applications

According to the definition of CSW and non-CSW residual in PCCF, this section shows some examples and potential applications of the CSWs and the non-CSW residual separately. The demonstration reflects both the validity and practicability of the proposed extraction approach.

A. The CSWs

Since CSWs are essentially caused by the catenary structure where the PCCF signal is measured from, it ought to change with the specific parameters of catenary structure. Once the catenary structure is determined, the speed and type of pantograph should not influence the frequency characteristic of CSW, although they may alter the amplitude of CSW. Considering PCCF can be measured from different pantograph-catenary interaction under various operation conditions, it is crucial for the extracted CSWs to be consistent and only sensitive to corresponding structure parameters. Otherwise, the CSWs cannot be useful for reflecting the overall quality of interaction. Thus, the following three cases intend to

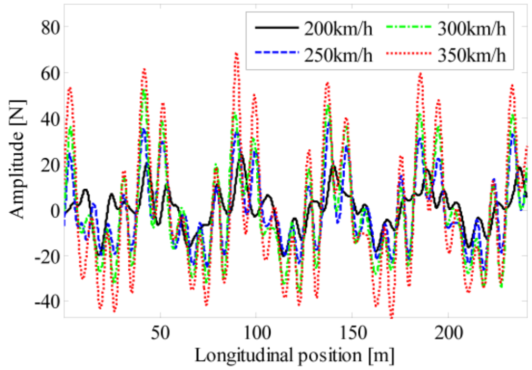

Fig. 11. Extracted CSWs of PCCF under different operation speed in Case 1.

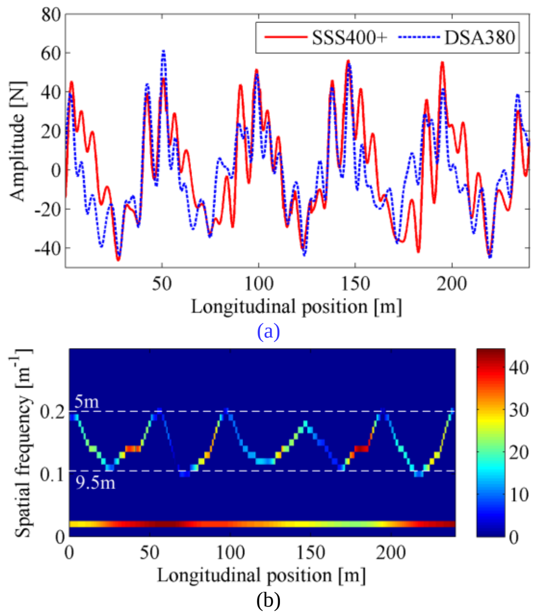

Fig. 12. (a) Extraction result comparison and (b) CSWs spectrum in Case 2.

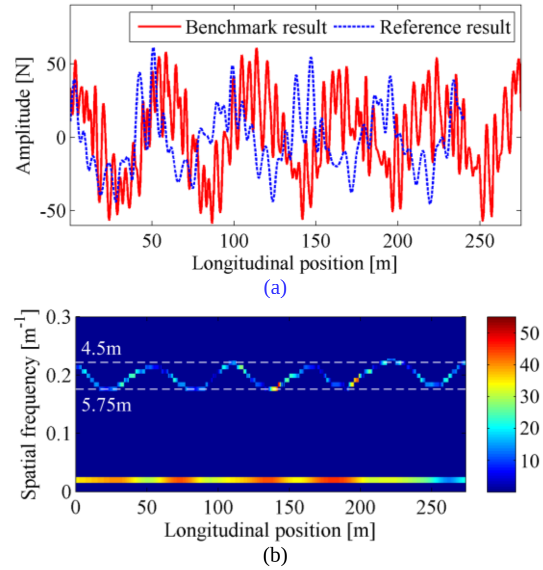

Fig. 13. (a) Extraction result comparison and (b) CSWs spectrum of the benchmark simulation in Case 3.

show that the extraction approach is functioning properly as expected. The 5-span PCCF signal depicted in Fig. 4(a) and its extraction results are adopted as a reference for comparisons.

Case 1, Operation speed: In this case, the PCCF signals adopted for extraction are from the same simulation as the reference but with different operation speed. Fig. 11 depicts the extracted CSWs of four PCCF signals under operation speed 200km/h, 250km/h, 300km/h and 350km/h, respectively. It can be observed that, with the increase of operation speed, the amplitude of CSWs becomes larger due to the higher vibration between pantograph and contact wire. However, the peaks and valleys of the oscillations appear at the same or adjacent positions, which indicate that the periodicity of CSWs remains similar despite of the change of speed. Thus, it shows that the extraction approach works properly under different operation speed. Note that for the PCCF signals measured under nonconstant operation speed, the extraction approach can still be functional because the instantaneous frequencies of CSWs remain unaffected and can be recognized by (9).

Case 2, Pantograph type : In this case, the PCCF signal is from the same simulation as the reference, but using the SSS400+ pantograph given in Table II instead of the DSA380 pantograph. Fig. 12(a) depicts the comparison between the extracted CSWs from the two types of pantograph. The new CSWs generated by SSS400+ pantograph are similar in general to the CSWs of the reference, but different at some locations due to the differences of the physical parameters of the pantographs. From the Hilbert spectrum of the new CSWs depicted in Fig. 12(b), it can be seen that, comparing with the reference spectrum in Fig. 8(a), the instantaneous frequencies of CSWs are within the same and valid frequency range. However, the frequency deviation in TFD is more severe than the reference TFD, namely the new TFD is less similar to the ideal TFD of catenary structure in Fig. 8(b) than the reference. Considering the definition of CSW, since the reflection of catenary structure in the new PCCF is weakened, this phenomenon can be regarded as a sign of less favorable pantograph-catenary contact quality. The same conclusion can be drawn by comparing the means and standard deviations of the new and reference PCCF signals. Concretely, the means are 155.3N and 155.2N respectively and nearly identical, whereas the standard deviations are 33.8N and 40.7N respectively, which indicate a relatively unfavorable contact quality in case of SSS400+ pantograph.

Case 3, Catenary structure: In this case, two PCCF signals from completely different pantograph-catenary interactions are adopted for extraction. The first one is the simulation result based on the benchmark model given in [24]. The other is from a real-life PCCF measurement data in a section of the Shanghai-Kunming railway line in China.

In the benchmark model, the main structure parameters of catenary, namely the span is 55m, and the inter-dropper distance is 4.5m at both ends of a span and 5.75m in the middle of a span. Other simulation parameters such as operation speed, sampling interval, total number of spans and so on are all the same. Likewise, the 5-span PCCF signal at the same location in the middle of catenary model is adopted for extraction, whose duration is 35m longer than the reference. As a result, the CSWs and non-CSW residual are depicted in Fig. 13(a). It can be seen that, due to the difference of spans, the overall trends of the CSWs have a certain phase difference. Meanwhile, because

Please cite as: Z. Liu, H. Wang, R. Dollevoet, Y. Song, A. Núñez, J. Zhang, "Ensemble EMD-based automatic extraction of the catenary structure wavelength from the pantograph-catenary contact force". Accepted IEEE Transactions on Instrumentation and Measurement, Jun. 2016. DOI: 10.1109/TIM.2016.2579360

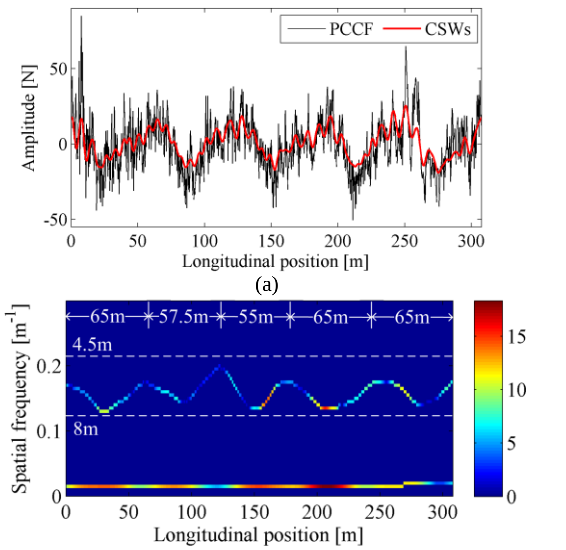

(b)

Fig. 14. (a) The mean-removed PCCF measurement data comparing with its CSWs and (b) the CSWs spectrum of the PCCF in Case 3.

there are four more droppers in each span of the benchmark model than in the reference model, the oscillations of CSWs in one span is clearly more intensive than the reference CSWs. Therefore, in the corresponding Hilbert spectrum depicted in Fig. 13(b), the instantaneous frequencies reflecting the inter-dropper distances oscillate within a relatively narrow frequency band that ranges from 4.5m to 5.75m in wavelength. In general, the extraction approach shows certain adaptability to the variation of catenary structure and pantograph parameters.

In the other trial, a segment of PCCF measurement data with 307.5m duration and 0.5m sampling interval is analyzed. The PCCF signal is obtained from an inspection locomotive with pressure and acceleration sensors installed under the contact strip of the pantograph. During the measuring process, the operation speed is consistent and approximately 125km/h. There are five spans in the section where the PCCF is measured, which are 65m, 57.5m, 55m, 65m and 65m long, respectively. Along the five spans, the droppers are unevenly distributed along the five spans and served a long-term operation. The inter-dropper distances range from 4.5m to 8m approximately. Fig. 14(a) depicts the PCCF measurement data with 98.9N mean removed and its corresponding CSWs. As a result of the extraction approach, the CSWs favorably exclude the interference of several abnormally high forces and fit the overall trend of PCCF. The result indicates that the non-CSW residual contains the abnormal signal components in the PCCF measurement data. Meanwhile, the amplitude of the CSWs ranges from -15N to 15N that is much lower than the amplitude of the reference CSWs in Fig. 9 due to the lower operation speed. It agrees with the discussion regarding the operation speed in Case 1. Furthermore, from the Hilbert spectrum of the CSWs depicted in Fig. 14(b), it can be seen that the instantaneous frequencies reflecting the inter-dropper distances oscillate in the actual span cycles in longitudinal direction and between 4.5m and 8m wavelengths in spatial frequency, which

TABLE III
VARIATION COEFFICIENTS UNDER THE CONTAMINATIONS OF NOISE WITH DIFFERENT SNR

SNR (dB)	0.1	0.2	0.5	1	2	5	10	20
Variation coefficient (%)	4.9	4.8	4.6	4.4	4.2	3.3	2.3	1.5

meets the expectation of the frequency-domain characteristics of CSWs. Although the energy distribution in the spectrum is less regular comparing with the ones from simulation data due to complex measurement conditions, the extraction approach still produces the correct results.

To sum up, the proposed extraction approach could be functional for most PCCF signals. Meanwhile, as the dominant energy component in PCCF, the extracted CSWs can reflect the overall trend of PCCF signal in both amplitude and frequency adequately. Note that if certain anomaly happens to excites the frequency component within the frequency range of CSWs, the amplitude and energy of the CSWs will be higher than usual, which can be an indicator of the anomaly.

B. The Non-CSW Residual

The non-CSW residual of a PCCF signal is mainly the combined result of high-frequency vibration, measurement noise, environmental disturbance and other possible anomalies in pantograph-catenary system. Since it is essentially the PCCF residual with the elimination of CSWs, it can facilitate the analysis of signal components that are not dominant in PCCF, which contain most hidden information on early-stage anomalies or potential threats to the pantograph-catenary interaction. Tentatively, the following examples show the potential applications of non-CSW residual in the aspects of noise tolerance and anomaly detection.

1) Noise tolerance: with the capability given by EEMD, the extraction approach can preserve the CSWs from the contamination of measurement noise. In other words, the non-CSW residual shall automatically contain most of the measurement noise, if there is any. Thus, the measurement noises caused by different PCCF measuring system can hardly affect the extraction results.

Using the same reference PCCF signal depicted in Fig. 4(a), white Gaussian noise series with different signal-to-noise power ratio (SNR) are added to the signal to test the tolerance of extraction approach against noise. To quantify the effect of noise on the extraction result, a variation coefficient is defined as

$$V=\frac{\frac{1}{T}\sum_{t=0}^{T}\left|CSW_n(t)\text{-}CSW_r(t)\right|}{\max[CSW_r(t)]-\min[CSW_r(t)]}\times 100\% \qquad (10)$$

where $CSW_n(t)$ and $CSW_r(t)$ are the extracted CSWs from the PCCF signals with and without additive noise, respectively, and T is the total duration of the CSWs. The variation coefficient calculates the average shifting rate of CSWs comparing with noise-free CSW.

To show the approach performances under low and high SNR noises in different measurement condition, the adopted SNRs of noise range from 0.1dB to 20dB. Table III presents the average variation coefficient of 20 trials for each SNR

Please cite as: Z. Liu, H. Wang, R. Dollevoet, Y. Song, A. Núñez, J. Zhang, “Ensemble EMD-based automatic extraction of the catenary structure wavelength from the pantograph-catenary contact force”. Accepted IEEE Transactions on Instrumentation and Measurement, Jun. 2016. DOI: 10.1109/TIM.2016.2579360

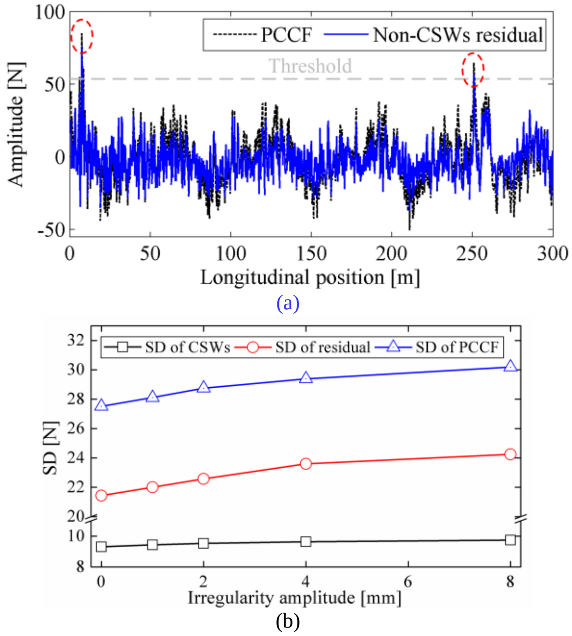

Fig. 15. (a) The mean-removed PCCF measurement data and its non-CSW residual. (b) Comparisons of the standard deviations (SDs) of PCCF, CSWs and non-CSW residual with respect to the irregularity amplitude.

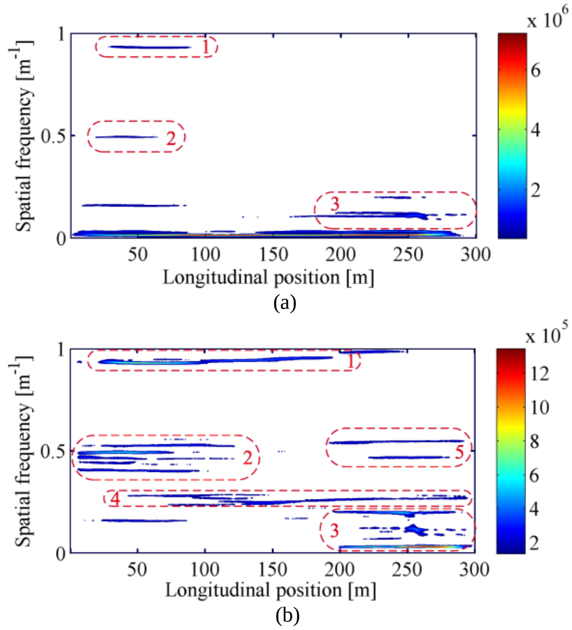

Fig. 16. Quadratic TFRs of (a) the mean-removed PCCF measurement data and (b) the corresponding non-CSW residual.

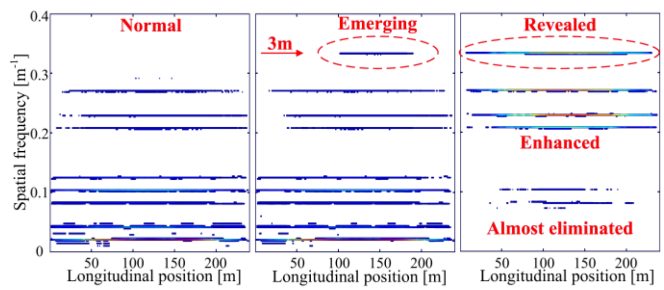

Fig. 17. Quadratic TFRs of the healthy PCCF (left), the unhealthy PCCF (middle) and the non-CSW residual of unhealthy PCCF (right).

respectively. The variation coefficient remains below 5% at low SNRs, which rarely exist in real-life PCCF measurements. Considering the pressure or acceleration sensor employed in PCCF measurement commonly has the capability to keep the output SNR above 5dB, which is equivalent to 3.3% variation coefficient at most, the influence of measurement noise on the extraction approach could be negligible. Actually, it enhances the practicability of the extraction approach.

2) Anomaly detection: normally, the catenary anomaly cannot influence the CSWs in PCCF since the catenary structure can hardly be altered and the energy of CSWs is too high to be submerged by anomalies. The non-CSW residual can usually preserve the signal components indicating anomalies. As examples, the PCCF measurement data depicted in Fig. 14(a) and some simulation PCCF data under contact wire irregularity are discussed below with the help of the quadratic time-frequency representation (TFR) for PCCF analysis [22].

In the time domain, the non-CSW residual contains most of the concerned statistical characteristics in the original PCCF, such as abnormal sample point and high standard deviation. Using the same PCCF measurement data depicted in Fig. 14(a), Fig. 15(a) depicts the PCCF with mean removed and its corresponding non-CSW residual. When evaluating the amplitude of PCCF, there is a common threshold criterion that considers the PCCF exceeding three times of the standard deviation as an abnormal sample point. Thus, two abnormal points are obtained by the criterion as circled by the dashed red line in the figure. After the extraction, the non-CSW residual clearly preserves the two abnormal points and keeps the corresponding CSWs unaffected as well. For comparison purposes, some simulation PCCF data from [22] are adopted, in which the contact wire irregularities simulated by 3m-wavelength cosine waveform with 1mm to 8mm amplitude are added to the contact wire. Fig. 15(b) depicts the standard deviations of the simulation PCCF, the corresponding CSWs and non-CSW residual. It can be observed that as the irregularity amplitude increases, the standard deviation of PCCF becomes higher, which indicates the deterioration of contact quality. As for the extraction results, while the standard deviations of CSWs remains almost constant for all amplitudes, the standard deviations of non-CSW residual show the same increasing trend as the standard deviations of original PCCF. Thus, the extracted non-CSW residual can also preserve the fluctuation characteristic of PCCF properly.

In the frequency domain, Fig. 16(a) and (b) depicts the TFRs of the two signals in Fig. 15(a). In the TFR of PCCF, the energy of CSWs is so large that submerges other signal components and leads to most energy locating at around the span wavelength. But in the circled and numbered region 1, 2 and 3 in Fig. 16(b), there are still signs of other component exist. In the TFR of the non-CSW residual depicted in Fig. 16(b), the energy of CSWs at the bottom is eliminated and the signal components in region 1, 2 and 3 are somehow fully revealed and enhanced. In addition, some emerging signal components appear at region 4 and 5. It should be noted that the enhanced or emerging components are not necessarily representing anomalies, because they may be caused by high-frequency vibration and environmental disturbance too. The precise anomaly detection depends on prior information of the normal or previous components in PCCF. Take the PCCF adopted in Fig. 15(b) as an example, the simulation PCCF signal, namely the unhealthy PCCF signal under the global contact wire irregularity with 3m wavelength and 8mm amplitude is analyzed. The PCCF signal is the exact same one as in [22] to demonstrate the advantage of proposed method. Note that in the simulation, the contact wire irregularity is controlled to be the only existing anomaly to test the performance of the extraction approach. In Fig. 17, the quadratic TFRs of the healthy PCCF, the unhealthy PCCF and the non-CSW residual of unhealthy PCCF are depicted in the left, middle and right, respectively. The color bar of TFR is not given for simplicity. Comparing the middle TFR with the left one, the unhealthy PCCF is influenced by the contact wire irregularity that leads to an emerging signal component appearing at the corresponding wavelength of 3m. However, as circled by the dashed line, the component is weak in energy and short in duration, which does not meet the fact that the contact wire irregularity is a global one throughout the entire longitudinal position. In the TFR of non-CSW residual on the right, it can be seen that the low-frequency part of unhealthy PCCF is mostly eliminated after the extraction. Consequently, the part above $0.2m^{-1}$ spatial frequency is largely enhanced, particularly the signal component that indicates the global irregularity as circled by the dashed line. Therefore, the employment of non-CSW residual can certainly be helpful to reveal the submerged components and make the anomalies easier to detect.

V. Conclusion and Outlook

This paper presents a new signal extraction approach specifically aiming at the dominant signal component, namely the CSW in PCCF generated by the interaction between soft catenary suspension and pantograph. The concept of CSW is described based on a theoretical study on pantograph-catenary interaction. To extract the CSWs automatically, the data-driven EEMD algorithm is employed to decompose the PCCF signal with proper boundary extension. Thereupon, the extraction of CSWs and non-CSW residual is realized by utilizing the property that all the decomposed signal components occupy non-overlapping frequency bands. The preliminary results based on simulation and measurement data indicate that the extraction approach is adaptive to various sources of PCCF with high tolerance against measurement noise and effective preservation of the catenary anomalies. Some potential applications of the extracted CSWs and non-CSW residual of PCCF are also suggested for further developments. As for the real-time application of the extraction approach in an on-board measuring system, assuming the extraction will be performed every 5 spans, which is equivalent to about every 3 seconds in an operation under 300km/h speed, the time duration is more than sufficient for the EEMD-based extraction with 100 ensemble members according to the EEMD implementation on a laptop with 2.4 GHz GPU [33].

In future studies concerning the evaluation of current collection quality, the extraction approach could be a useful substitute for the conventional method that usually performs a filter with cut-off frequency 20Hz on a PCCF signal to obtain the low-frequency component of PCCF. It is more accurate comparing with the partial elimination and preservation of the full frequency band of PCCF. Meanwhile, the non-CSW residual of PCCF can facilitate anomaly detections, especially early-stage anomalies that may be submerged by CSWs.

Acknowledgment

The authors would like to thank the anonymous reviewers for their valuable comments.

References

[1] M. Givoni, "Development and impact of the modern high-speed train: A review," *Transport Rev.*, vol. 26, no. 5, pp. 593–611, Sep. 2006.
[2] W. Zhang, Z. Shen, and J. Zeng, "Study on dynamics of coupled systems in high-speed trains," *Veh. Syst. Dyn.*, vol. 51, no. 7, pp. 966-1016, Jun. 2013.
[3] Y. Song, Z. Liu, H. Wang, X. Lu, and J. Zhang, "Nonlinear modelling of high-speed catenary based on analytical expressions of cable and truss elements," *Veh. Syst. Dyn.*, vol. 53, no. 10, pp. 1455-1479, Jun. 2015.
[4] B. Allotta, L. Pugi, and F. Bartolini, "Design and experimental results of an active suspension system for a high-speed pantograph," *IEEE/ASME Trans. Mechatronics*, vol. 13, no. 5, pp. 548-557, Oct. 2008.
[5] *Railway Applications—Current Collection Systems—Requirements for and Validation of Measurements of the Dynamic Interaction Between Pantograph and Overhead Contact Line*, GEL/9/3 Std. BS EN 50317, 2002.
[6] A. Facchinetti and M. Mauri, "Hardware-in-the-loop overhead line emulator for active pantograph testing," *IEEE Trans. Ind. Electron.*, vol. 56, no. 10, pp. 4071-4078, Oct. 2009.
[7] S. M. Mousavi, A. Tabakhpour, E. Fuchs, and K. Al-Haddad, "Power quality issues in railway electrification: A comprehensive perspective," *IEEE Trans. Ind. Electron.*, vol. 62, no. 5, pp. 3081–3090, May 2015.
[8] G. Bucca and A. Collina, "A procedure for the wear prediction of collector strip and contact wire in pantograph–catenary system," *Wear*, vol. 266, no.1, pp. 46-59, Jan. 2009.
[9] S. Jung, Y. Kim, J. Paik, and T. Park, "Estimation of dynamic contact force between a pantograph and catenary using the finite element method," *J Comput. Nonlinear Dyn.*, vol. 7, no. 4, pp. 041006, Jun. 2012.
[10] J. Kim, H. Chae, B. Park, S. Lee, C. Han, and J. Jang, "State sensitivity analysis of the pantograph system for a high-speed rail vehicle considering span length and static uplift force," *J. Sound Vibration*, vol. 303, no. 3, pp. 405-427, 2007.
[11] O. V. Van, J. Massat, C. Laurent, and E. Balmes, "Introduction of variability into pantograph-catenary dynamic simulations," *Veh. Syst. Dyn.*, vol. 52, no. 10, pp. 1254-1269, Aug. 2014.
[12] W. Zhang, Y. Liu, and G. Mei, "Evaluation of the coupled dynamical response of a pantograph-catenary system: contact force and stresses," *Veh. Syst. Dyn.*, vol. 44, no. 8, pp. 645-658, Aug. 2006.
[13] J. Kim, "An experimental study of the dynamic characteristics of the catenary-pantograph interface in high speed trains," *J. Mech. Sci. and Tech.*, vol. 21, no. 12, pp. 2108-2116, Dec. 2007.
[14] A. Collina, F. Fossati, M. Papi, and F. Resta, "Impact of overhead line irregularity on current collection and diagnostics based on the measurement of pantograph dynamics," *Proc. IMechE Part F: J. Rail Rapid Transit*, vol. 221, no. 4, pp. 547-559, 2007.
[15] S. Kusumi, T. Fukutani, and K. Nezu, "Diagnosis of overhead contact line based on contact force," *Quart. Rep. of RTRI*, vol. 47, no. 1, pp. 39-45, Feb. 2006.
[16] I. Aydin, M. Karakose, and E. Akin, "Anomaly detection using a modified kernel-based tracking in the pantograph–catenary system," *Expert Syst. With Applic.*, vol. 42, no. 2, pp. 938-948, Feb. 2015.
[17] J. Pombo, J. Ambrósio, M. Pereira, F. Rauter, A. Collina, and A. Faccinetti, "Influence of the aerodynamic forces on the pantograph–catenary system for high-speed trains," *Veh. Syst. Dyn*, vol. 47, no. 11, pp. 1327-1347, Oct. 2009.
[18] B. Peng, X. Wei, B. Deng, H. Chen, Z. Liu, and X. Li, "A Sinusoidal Frequency Modulation Fourier Transform for Radar-Based Vehicle Vibration Estimation," *IEEE Trans. Instrum. Meas.*, vol. 63, no. 9, pp. 2188-2199, Sep. 2014.

[19] S. Banerjee and M. Mitra, "Application of cross wavelet transform for ecg pattern analysis and classification," *IEEE Trans. Instrum. Meas.*, vol. 63, no. 2, pp. 326-333, Feb. 2014.
[20] N. E. Huang *et al.*, "The empirical mode decomposition and the Hilbert spectrum for nonlinear and non-stationary time series analysis," *Proc. Roy. Soc. London A*, vol. 454, pp. 903–995, Mar. 1998.
[21] Z. Wu and N. E. Huang, "Ensemble empirical mode decomposition: a noise-assisted data analysis method," *Adv. Adapt. Data Anal.*, vol. 1, no. 1, pp. 1-41, 2009.
[22] H. Wang, Z. Liu, Y. Song, X. Lu, Z. Han, J. Zhang, and Y. Wang, "Detection of contact wire irregularities using a quadratic time-frequency representation of the pantograph-catenary contact force," *IEEE Trans. Instrum. Meas.*, vol. 65, no. 6, pp. 1385-1397, Jun. 2016.
[23] *Railway Applications—Current Collection Systems—Validation of Simulation of the Dynamic Interaction Between Pantograph and Overhead Contact Line*, European Standard EN 50318, Jul. 2002. CENELEC, European Committee for Electrotechnical Standardization.
[24] S. Bruni, J. Ambrosio, A. Carnicero, Y. H. Cho, L. Finner, M. Ikeda, S. Y. Kwon, J. Massat, S. Stichel, M. Tur, and W. Zhang, "The results of the pantograph–catenary interaction benchmark," *Veh. Syst. Dyn.*, vol. 53, no. 3, pp. 412-435, Jun. 2015.
[25] N. Tsakalozos, K. Drakakis, and S. Rickard, "A formal study of the nonlinearity and consistency of the empirical mode decomposition," *Signal Process.*, vol. 92, no. 9, pp. 1961-1969, Sep. 2012.
[26] R. Li and D. He, "Rotational machine health monitoring and fault detection using EMD-based acoustic emission feature quantification," *IEEE Trans. Instrum. Meas.*, vol. 61, no. 4, pp. 990-1001, Apr. 2012.
[27] P. Flandrin, G. Rilling, and P. Goncalves, "Empirical mode decomposition as a filter bank," *IEEE Signal Process. Lett.*, vol. 11, no. 2, pp. 112–114, Feb. 2004.
[28] N. Chatlani and J. J. Soraghan. "EMD-based filtering (EMDF) of low-frequency noise for speech enhancement," *IEEE Trans. Audio, Speech Lang. Process.*, vol. 20, no. 4, pp. 1158-1166, May 2012.
[29] F. Bao, X. Wang, Z. Tao, Q. Wang, and S. Du, "EMD-based extraction of modulated cavitation noise," *Mech. Syst. Signal Proc.*, vol. 24, no. 7, pp. 2124-2136, Oct. 2010.
[30] A. O. Boudraa and J. C. Cexus. "EMD-based signal filtering," *IEEE Trans. Instrum. Meas.*, vol. 56, no. 6, pp. 2196-2202, Dec. 2007.
[31] A. Komaty, A. O. Boudraa, B. Augier, and D. Daré-Emzivat, "EMD-based filtering using similarity measure between probability density functions of IMFs," *IEEE Trans. Instrum. Meas.*, vol. 63, no. 1, pp. 27-34, Jan. 2014.
[32] N. E. Huang and S. S. P. Shen, Eds., *Hilbert-Huang Transform and Its Applications*. Singapore: World Scientific, 2005.
[33] Y. H. Wang, C. H. Yeh, H. W. V. Young, K. Hu, and M. T. Lo, "On the computational complexity of the empirical mode decomposition algorithm," *Physica A*, vol. 400, pp. 159–167, 2014.

Zhigang Liu (M'06–SM'16) received the Ph.D. degree in power system and automation from the Southwest Jiaotong University, Chengdu, China, in 2003.
He is currently a Full Professor with the School of Electrical Engineering, Southwest Jiaotong University. His current research interests include electrical relationship of vehicle-grid in high-speed railway, power quality considering grid-connect of new energies, pantograph-catenary dynamic, and fault detection, status assessment and active control.

Hongrui Wang (S'15) received the B.S. degree in electrical engineering and automation from Mao Yisheng Class, Southwest Jiaotong University, Chengdu, China, in 2012, where he is currently pursuing the Ph.D. degree with the School of Electrical Engineering.
He is currently involved in a Joint PhD Program sponsored by the China Scholarship Council with the Section of Railway Engineering, Delft University of Technology, Delft, The Netherlands. His research interests include signal decomposition, time-frequency analysis, signal filtering, machine learning and their applications in the assessment, detection, diagnosis and maintenance of railway pantograph-catenary system.

Rolf Dollevoet received the M.Sc. degree in mechanical engineering from Eindhoven University of Technology, Eindhoven, The Netherlands, and the Ph.D. degree from the University of Twente, Enschede, The Netherlands, in 2010.
Since 2003, he has been with ProRail, Utrecht, The Netherlands. Since 2012, he has been appointed as a part-time Professor with the Section of Railway Engineering, Delft University of Technology, Delft, The Netherlands. He is also currently the leader of scientific research on rolling contact fatigue and wheel–rail interface within ProRail Civil Engineering and the Chair of the International Union of Railways working group on wheel–rail conditioning and lubrication.
Dr. Dollevoet was a recipient of the Jan van Stappen Spoorprijs 2010 Award (a yearly prize for contributions to the travel quality and service for passengers in The Netherlands) from the railway sector for his Ph.D. research and its huge potential to reduce track maintenance costs.

Yang Song (S'16) received the B.S. degree in mechanical engineering from Shanghai University of Electric Power, Shanghai, China, in 2011. He is currently pursuing the Ph.D. degree with the School of Electrical Engineering, Southwest Jiaotong University.
He is currently involved in a Joint PhD Program sponsored by the China Scholarship Council with the School of Engineering, University of Liverpool, Liverpool, The United Kingdom. His research interests include modeling and aerodynamic of the pantograph-catenary system, and active control of the pantograph.

Alfredo Núñez (M'02–SM'14) received the Ph.D. degree in electrical engineering from the Universidad de Chile, Santiago, Chile, in 2010.
He was a Postdoctoral Researcher with the Delft Center for Systems and Control. He is currently with the Section of Railway Engineering, Delft University of Technology, Delft, The Netherlands. He authored the book Hybrid Predictive Control for Dynamic Transport Problems in the Series of Advances in Industrial Control (Springer-Verlag, 2013). His research interests include monitoring and maintenance of railway infrastructure, modeling and control of traffic and transportation systems, model predictive control, and fuzzy systems.

Jing Zhang received the Ph.D. degree in mechanical manufacturing engineering and automation from Southwest Jiaotong University, Sichuan, China, in 2008.
She is currently an Associate Professor with the School of Electrical Engineering, Southwest Jiaotong University. Her research interests include optimization design of pantograph-catenary parameters, aerodynamics of pantograph-catenary system and control technology of high-speed pantograph.